

# Large Wave Characteristics and Their Downstream Evolution at High Reynolds Number Falling Films

Margaritis Kostoglou, Konstantinos Samaras, and Thodoris D. Karapantsios  
Div. of Chemical Technology, Dept. of Chemistry, Aristotle University of Thessaloniki,  
54124 Thessaloniki, Greece

DOI 10.1002/aic.11992

Published online August 24, 2009 in Wiley InterScience (www.interscience.wiley.com)

*There are many open questions regarding the evolution of waves, especially for the case of turbulent films. To resolve the complexity in modeling wavy turbulent films, more information needs to be derived from experimental data. On this account, a new way is proposed herein to analyze experimental film thickness traces, replacing the usual statistical analysis. Large waves are identified in experimental traces, and their shape is described by approximation with a few parameters curve. The probability density functions of these parameters are identified and the whole procedure can be considered as a compression method of the information content of experimental data series. By comparing results at several downstream locations, information on the evolution of waves along the flow is derived. This information indicates a 3D character of the flow, customary neglected in modeling efforts. In addition, the current results can be used for the numerical reconstruction of experimental film thickness traces. © 2009 American Institute of Chemical Engineers AIChE J, 56: 11–23, 2010*

*Keywords: falling film, wave characterization, surface morphology, statistical analysis*

## Introduction

Thin film flow occurs in several industrial processes such as falling film reactors and evaporators, gas absorption towers, and direct contact condensation units.<sup>1,2</sup> The optimal design and operation of these apparatuses requires understanding of the underlying transport processes. This is by no means a straightforward task due to the well-known hydrodynamic instability, which manifests itself in the form of surface waves. Although waves in an industrial process can be produced by the influence of a concurrent/countercurrent gas flow or by physical obstacles, the inherently unstable free falling film—presenting waves at no gas flow—apart from its direct practical significance serves as a classical hydrodynamic problem of fundamental interest for the study of wave's dynamics.<sup>3,4</sup> The waves appearing on the surface

of the film are known to enhance the mass and heat transfer not only in a static way (i.e., increasing the contact area between the gas and liquid phase) but chiefly in a dynamic way by creating transverse velocity fields (perpendicular to main film flow) in both phases. Therefore, the need for studying the hydrodynamics of falling films is evident. The wave structure is an important part of this hydrodynamics.

There have been many experimental studies measuring mainly the time evolution of liquid film thickness at specific locations along the flow using several measurement techniques. The majority of these studies sought only integral statistical properties of the wavy film thickness traces such as mean value, standard deviation, maxima and minima values, probability density functions of film thickness, dominant wave frequencies by Fourier analysis, average wave velocities by cross-correlating simultaneous data from neighboring locations,<sup>5–8</sup> and did not bother about recognizing and analyzing individual waves. However, the dynamics of waves is chaotic and therefore the above statistical quantities delivering integral information over a time period cannot help in

Correspondence concerning this article should be addressed to T. D. Karapantsios at karapant@chem.auth.gr

understanding the structure of the surface. There are fewer studies focusing on the measurement of the velocity profile within the laminar wavy film.<sup>9,10</sup>

Theoretical approach (numerical solution of the governing equations) appears as a promising way to gain insight on the flow structure. Although the complete mathematical problem based on the Navier-Stokes equation with the appropriate free surface boundary conditions can be easily formulated, its solution along the film flow is computationally very intensive. For this, several approximate techniques have been developed over the years. An additional complication arises from the fact that as Reynolds number increases, the flow inside the film first gets transitional and then turbulent. Most of the experimental and almost all theoretical works are limited to the case of laminar films. The solution of the mathematical problem even for laminar flow requires geometry simplification or equations simplification. The geometry simplification includes solution of the equations for the flow field in a wave of specified shape (usually determined experimentally<sup>11</sup>) or the solution of the complete equations for the evolution of waves in restricted (periodic<sup>12,13</sup> or truncated<sup>14</sup>) domains. In some cases, problems with artificial initial conditions are studied.<sup>15</sup> A different approach is the solution of reduced equations in the real geometry. The so-called long-wave equation<sup>16</sup> based on the lubrication approximation for the local velocity profile has been developed for this purpose. Extensions of this approach leaving as unknown the velocity profile are the boundary layer equation<sup>17</sup> and the second-order boundary layer equations.<sup>18</sup> These problems are solved numerically by expanding the velocity profile to a few polynomial modes. More recently, the advancement of techniques in the spirit of volume of fluid (VOF) has permitted the direct simulation of the evolution of falling films in two and even three dimensions using the complete Navier-Stokes equation.<sup>19–21</sup> For computational reasons, however, this approach is restricted to Reynolds numbers less than 100. Two-dimensional simulation of laminar falling films without assumptions has been also achieved recently using classical interface tracking techniques.<sup>22</sup>

In case of turbulent flow, the situation is exceedingly more complex. The more convenient approach is to ignore absolutely the morphology of waves and simply include their mixing effect into modified turbulent transport coefficients.<sup>23</sup> This seems naive at first sight but it is based on the fact that there may be no reason for detailed consideration of the waves given the uncertainty already introduced by the turbulence model. To our knowledge, the only attempt to model turbulent wavy falling film appears in Ye et al.<sup>24</sup> where the Reynolds Averaged Navier-Stokes together with a  $k-\varepsilon$  model are solved for the velocity field in a wave having an experimentally determined shape. It is important to note that as the  $Re$  number increases the simulation task becomes more difficult but on the contrary the experimental study becomes easier because of the thicker liquid films. So, it is desirable in this case to facilitate the simulation using experimental results.

It is apparent that more work is needed for the analysis of turbulent falling film hydrodynamics and its effect on transport processes. A different approach to extract information from film thickness data is followed here: the large (roll) waves, which represent the main feature of the film surface, are identified and then described one by one by an appropri-

ate function employing a few parameters. The statistics of these parameters are analyzed with respect to Reynolds number and downstream location. The outcome constitutes a reduced order description of the morphology of the surface. Such information can become the first step for the reconstruction of the surface shape of turbulent wavy films as proposed by Touglidis et al.<sup>25</sup> That study used wave data from just a single measuring location (2.5 m from liquid entry) and performed a simplified wave analysis having in mind more the efficiency of the reconstruction algorithm rather than the accuracy of wave data. As it was explained, the direct computation of the shape of the film surface is difficult, so a reconstructed surface (i.e., film thickness) evolution can be used in numerical codes for the computation of velocity fields and transport rates. It must be stressed that almost all the theoretical and most of the experimental work on falling film hydrodynamics is restricted to two dimensions (as this work) although there is evidence for the significance of the third dimension even for laminar falling films.<sup>26</sup>

The structure of this work is the following: at first, the experimental setup and procedure for receiving film thickness raw data at different downstream locations are presented. Then, the procedure of selecting large waves and analyzing their shape is described in detail. Finally, several results concerning statistics of wave shapes, temporal separation between waves and wave shape evolution along the main flow direction are presented and discussed with implications for their use in a surface reconstruction procedure.

## Experimental Part

The experimental setup is similar to that of Karapantsios and Karabelas.<sup>7</sup> The falling film is formed inside a vertical Plexiglass pipe of 0.05 m ID with 2.5 m total length. Specially constructed plugs mounted flush with the inner surface of the pipe at different downstream locations are used for measuring film thickness vs. time using the well-known parallel wire electrical conductance technique. For this, each plug is furnished with two parallel wires ( $\sim 0.5$  mm diameter,  $\sim 2$  cm length, and  $\sim 2$  mm apart in the horizontal direction) protruding laterally into the falling film. The plugs' downstream locations are 1.73, 1.83, 1.90, 2.00, 2.20, and 2.47 m, measured from the entry point. Because of end effects, data only from the upper five plugs are used in this study. Evidently, single-point film thickness measurements provide only a two-dimensional (2D) longitudinal representation of wave structures neglecting any 3D features in the angular direction.

Filtered, deaerated tap water at ambient conditions is used as the test liquid. A cylindrical vessel is used to introduce water by overflow at the top of the vertical pipe (located at the centerline of the vessel) forming a weir. To insure uniform film formation and a nearly flat surface (minimize disturbances) at the entrance, the weir is tapered over a length of  $\sim 10$  cm. Care is taken to minimize liquid agitation in the feeding vessel by using multiple liquid entry into it. Flexible hoses are used to suppress vibrations caused by the pump and hydraulic parts of the system. All the above are meant to suppress mechanically induced waves on the free surface of film. As a result, only physically excited waves (due to

hydrodynamic instabilities) are expected to develop along the flow.

Water from the vertical pipe exit freely into an open receiving vessel. Experiments are performed at temperature  $20^{\circ}\text{C} \pm 0.2^{\circ}\text{C}$  over a broad range of flow rates ( $803 \leq Re \leq 11,000$ ), which extends appreciably inside the turbulent flow regime. Reynolds number ( $Re$ ) is defined as  $4\Gamma/\mu$  where  $\Gamma$  is the liquid mass flow rate per unit width of wall and  $\mu$  is the liquid viscosity. Actually, there is no way to know at which region of  $Re$  number the transition from laminar to turbulent flow occurs without measuring the local velocity in the film. The problem is that the particular flow is inherently unstable and exhibits transient-chaotic behavior even in the laminar regime. The transition to turbulence manifests itself through an abrupt change of the frequency of the spatial and temporal velocity fluctuations. For the above reason, several values of  $Re$  number for the transition to turbulence can be found in literature (usually between 1000 and 4000). The only thing for which we can be sure of (according to literature) is that our experiments for  $Re > 4000$  are in the turbulent regime.

Data are collected with a 400 Hz sampling frequency, which was found adequate for capturing the features of such films. Three records of 5 s each are acquired at every flow rate (Reynolds number) and for all plug locations to check for repeatability and further increase the confidence of the calculated statistics. The estimated overall error in film thickness measurements including, calibration, measurement, digitization, and data handling is always less than 7%. The uncertainty in calculating the average wave velocity by cross correlating simultaneously acquired time records from different plugs depends on the spacing between plugs. For adjacent plugs the uncertainty never exceeds 5%.

## Data Processing

### Large wave selection

It is generally accepted that falling liquid films comprise mainly of (a) a very thin liquid substrate, which lies between the solid wall and surface waves; (b) large waves (also known as roll waves), which are surface undulations with height larger than the mean film thickness; and (c) ripples, which are surface undulations with height smaller than the mean film thickness, occupying the space between large waves. The first step of this work is the identification and isolation of large waves. Large waves are identified one by one from experimental records of local film thickness vs. time starting from the largest wave and continuing with the progressively smaller ones. The procedure was originally proposed by Touglidis et al.<sup>25</sup> but those authors stopped the identification when the selection reached the dominant wave frequency determined by FFT analysis. On the contrary, we continued the selection until all possible large waves have been accounted for. This allows a greater number of waves to be collected and so to improve the statistical significance of subsequent calculations.

### Reduced order representation and analysis of large waves

After the identification of large waves, the next step is their mathematical representation by a function with a

reduced set of parameters. The idea is of course not new, but the effort here is to find a function whose parameters are uncorrelated to each other and determine the probability density function (PDF) of the parameters. In general, if the shape of large waves is described by a function with  $n$  parameters, say  $F(t, a_1, a_2, \dots, a_n)$ , the distribution of these parameters can be described by a  $n$ -dimensional PDF, which requires an enormous number of wave data for its proper construction. On the other hand, in the particular case of uncorrelated parameters  $a_1, a_2, a_3, \dots$ , the following major simplification can be made

$$\text{PDF}(a_1, a_2, \dots, a_n) = \text{PDF}_1(a_1)\text{PDF}_2(a_2)\dots\text{PDF}_n(a_n)$$

permitting the simple construction of the individual probability density functions.

So, the scope is to find a function with the smallest number of uncorrelated parameters, which is capable to appropriately describe the measured shape of large waves. After a lot of trials, the following function emerged:

$$h = a + b \cdot \exp\left[-\frac{(c \cdot \ln \frac{t+e}{c})^2}{2w^2}\right] \quad (1)$$

the parameters  $a$  and  $b$  have length units whereas the parameters  $c$ ,  $e$ , and  $w$  have time units. The parameters  $a$  and  $e$  are auxiliary and serve only to justify properly the predicted with the experimental waves by adjusting the substrate thickness ( $a$ ) and shifting the time variable ( $e$ ) in order to achieve the best possible fitting. The effects of probable existence of smaller waves before or after large waves or the partial overlapping with other large waves are adsorbed in parameter  $a$ . The actual shape of the wave is described by the three parameters  $b$ ,  $c$ , and  $w$ . Parameter  $b$  depicts the amplitude (height) of the wave. Parameter  $c$  defines the time interval between the beginning of the wave and its peak (maximum) value. Finally, parameter  $w$  has not a direct physical meaning since the criterion for its selection was to be uncorrelated with the other parameters. Nevertheless, if we define the time-length  $P$  of a wave as the time span between the two points of the wave having height  $fb$  (where  $f$  is a small number chosen as 0.02 in this work), it is found that  $P$  can be determined from  $c$  and  $w$  as follows:

$$P = c \left[ e^{\left(\frac{w}{c}\sqrt{-2\ln f}\right)} - e^{-\left(\frac{w}{c}\sqrt{-2\ln f}\right)} \right] \quad (2)$$

The physical meaning of the mathematical parameters is shown graphically in Figure 1. The deviation between the experimental wave shape and its best fit with Eq. 1 is quantified through the fitting efficiency index  $R$ , which is computed as

$$R = 1 - \frac{\sqrt{\frac{\sum_{i=1}^n (h_{ir} - h_{is})^2}{n}}}{h_r} \quad (3)$$

where  $n$  is the number of experimental data points describing the wave,  $h_{ir}$  is the real (measured) height of wave at instant  $i$ ,

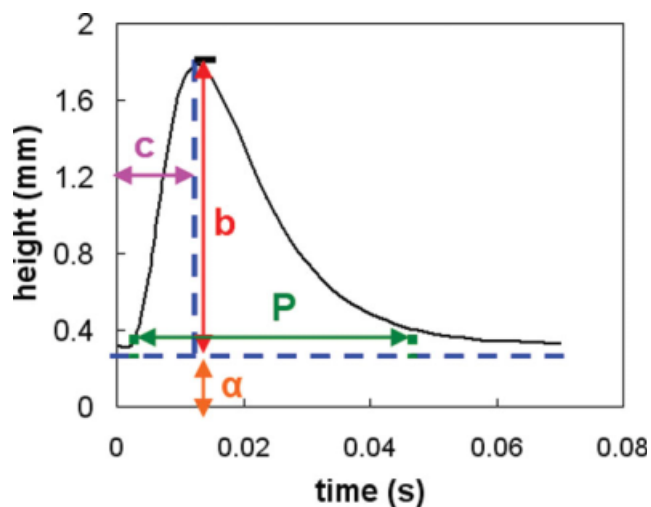


**Figure 1. Physical meaning of the parameters of Eq. (1) used to describe a wave.**

[Color figure can be viewed in the online issue, which is available at [www.interscience.wiley.com](http://www.interscience.wiley.com).]

$h_{is}$  is the simulated (fitted) height of wave at instant  $i$ , and  $h_r$  is the average experimental wave height.

All large waves (selected by only the height criterion) are fitted with Eq. 1. In some cases, the fitting was not good due to irregularities on a wave (humps or dents) or due to large overlapping of a wave with its neighboring wave(s). In any case, if the fitting criterion was  $<0.95$ , a wave was rejected. The quality of the fitting is generally high. The best and the worst fitting cases for all the waves examined in this work are shown in Figures 2a, b, respectively. Using this procedure, about 5% of the initially selected waves was excluded from the calculations of the statistics of the wave shape. The number of remaining waves varied with  $Re$  and downstream location but in general it was higher than the dominant frequency determined by FFT. The correlation between the fitting parameters is examined by cross plotting them. For instance, in Figure 3, it is evident that there is no correlation between the parameters  $c$  and  $w$  for the waves of the specific experimental trace.

The above type of functional representation of large waves was introduced by Touglidis et al.,<sup>25</sup> who proposed an algebraic function with four parameters where each one represented a different geometrical characteristic of the wave. Unfortunately, when we used their function to describe our waves, we discovered that two of their parameters were not entirely uncorrelated for an appreciable number of waves especially at Reynolds numbers above 5000. The above may, at least partly, explain why their reconstruction effort was unsuccessful above  $Re = 5000$ . Furthermore, Touglidis et al.<sup>25</sup> arbitrarily assumed the multidimensional PDF to be the product of uniform probability functions lying between two limiting (min, max) values. Herein, we have corrected and improved both these aspects. From the above, it is evident that the choice of the parameter triplet  $b, c, w$  is a crucial part of this work since it makes possible the construction of the three-dimensional (3D) PDF describing the wave characteristics.

## Results

### Large wave's characteristics at different downstream locations

Although the complete analysis has been performed for all examined downstream locations and Reynolds numbers, the presentation of all the results is not possible because of space limitations and hence only those necessary to support our arguments will be presented here. The evolution of the average wave characteristics along the flow (i.e., the degree of development of the flow) is addressed first. The evolution along the flow of the average value of the three wave shape parameters  $b, c, w$  is shown in Figures 4a–c, respectively. The bars denote the standard deviation of the corresponding PDFs at each downstream location. The figure refers to a particular Reynolds number but the general picture is the same for the other values of  $Re$ . It is apparent that virtually there are no detectable changes of the statistical

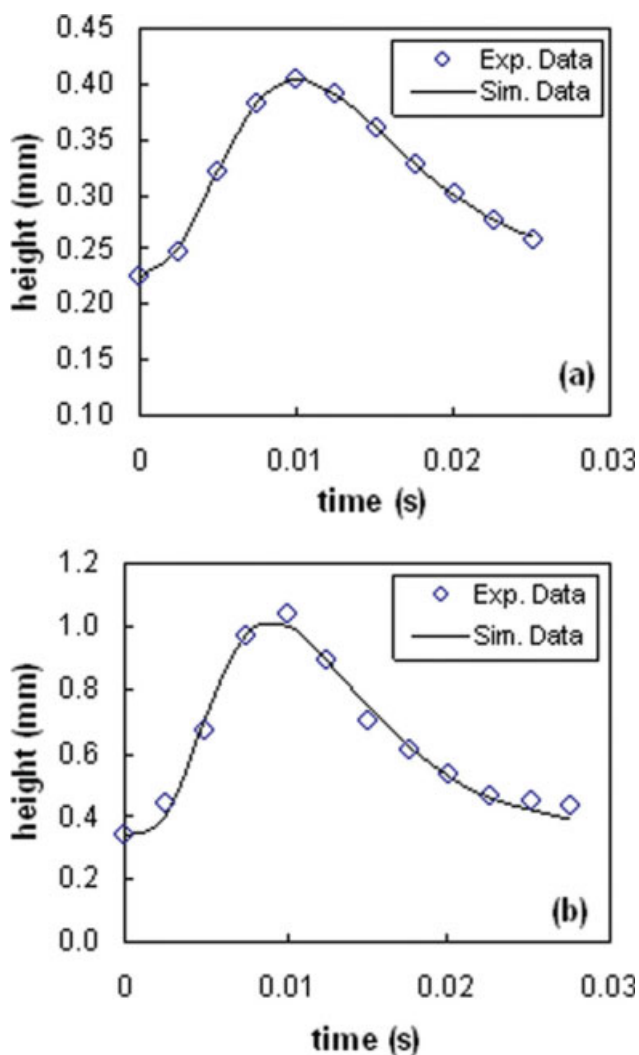


**Figure 2. (a) Best achieved fitting quality in this work ( $R = 0.997$ ) and (b) worst accepted fitting quality in this work ( $R = 0.955$ ).**

[Color figure can be viewed in the online issue, which is available at [www.interscience.wiley.com](http://www.interscience.wiley.com).]

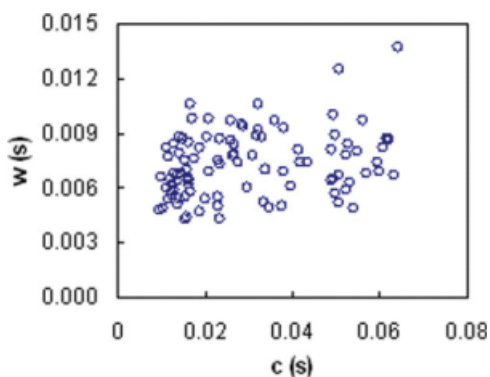


**Figure 3. A typical correlation plot between parameters  $c$  and  $w$ .**

[Color figure can be viewed in the online issue, which is available at [www.interscience.wiley.com](http://www.interscience.wiley.com).]

characteristics of the waves along the flow, so the flow in the region where the measurements were performed can be considered as fully developed.

The next step is to analyze the dependence of the average values of the wave shape parameters with respect to Reynolds number. Results are presented for a particular location (see Figure 5), but the behavior is the same for all the examined locations. For relatively low  $Re$  values, the average value of  $b$  increases with  $Re$  but it comes to saturation when  $Re$  exceeds 5000 (Figure 5a). If this is combined with the observed opposite trend for the minimum film thickness (not shown but well known in literature<sup>6</sup>), the following conclusion emerges: adding liquid to a low  $Re$  film, this goes mainly to large waves but adding liquid to a high  $Re$  film it goes mainly to the substrate. This description agrees with our earlier observations.<sup>27</sup> In Figures 5b,c, the dependence of parameters  $c$  and  $w$  on Reynolds number is presented. Given the stochastic nature of data, a relation between  $c$  or  $w$  with Reynolds number cannot be argued at any degree of significance.

Having a general idea of the dependence of wave shape parameters on downstream location and  $Re$ , let us get now a closer view of their PDF shape. Again, a dependence on location was not detected, so we will focus on the dependence on  $Re$  number. The PDF of parameter  $b$  for several Reynolds number is shown on Figure 6a. It is always unimodal and skewed toward large  $b$  for small  $Re$ . This skewness decreases as  $Re$  increases leading to symmetric distributions. It seems that there is a dramatic change in this parameter between  $Re = 3080$  and  $Re = 5290$  (unfortunately, there is no additional data in this region).

The PDF of parameter  $c$  vs. Reynolds number is shown in Figure 6b. These distributions are obviously bimodal implying the existence of two families of waves with different shape. There is a clear tendency of an increasing magnitude of the first mode and a decreasing magnitude of the second mode as  $Re$  increases. Except for the curve of  $Re = 830$ , all other curves are gathered together to the same envelope of curves. Because we care mainly for  $Re$  above 830, this envelope can be viewed as a master PDF that is followed by the parameter  $c$  for all high Reynolds number films. The same holds for parameter  $w$ . Its PDFs (see Figure 6c) do not show

any specific trend with respect to  $Re$ , so they can be considered as stochastic realizations of a master PDF. It is reminded that  $c$  is the time duration of the leading edge of

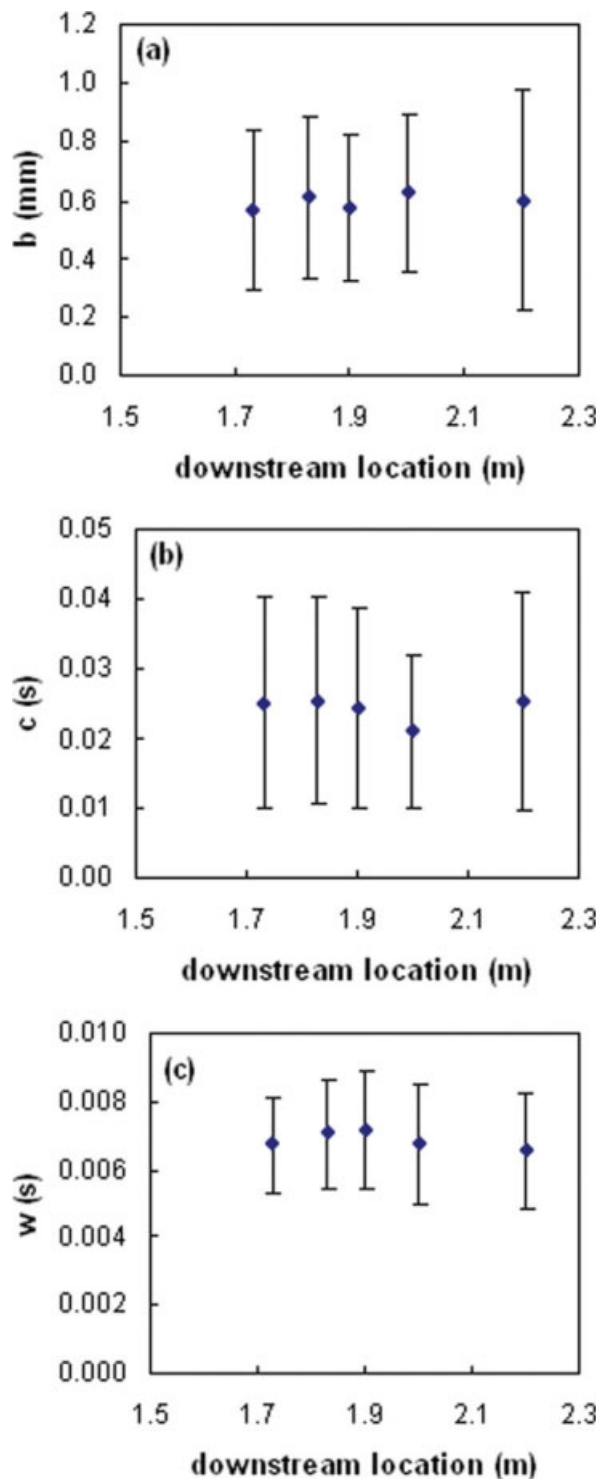


**Figure 4. Evolution of average value and standard deviation with downstream location of the wave shape parameters (a)  $b$ , (b)  $c$ , and (c)  $w$ . Data are for  $Re = 1160$ .**

[Color figure can be viewed in the online issue, which is available at [www.interscience.wiley.com](http://www.interscience.wiley.com).]

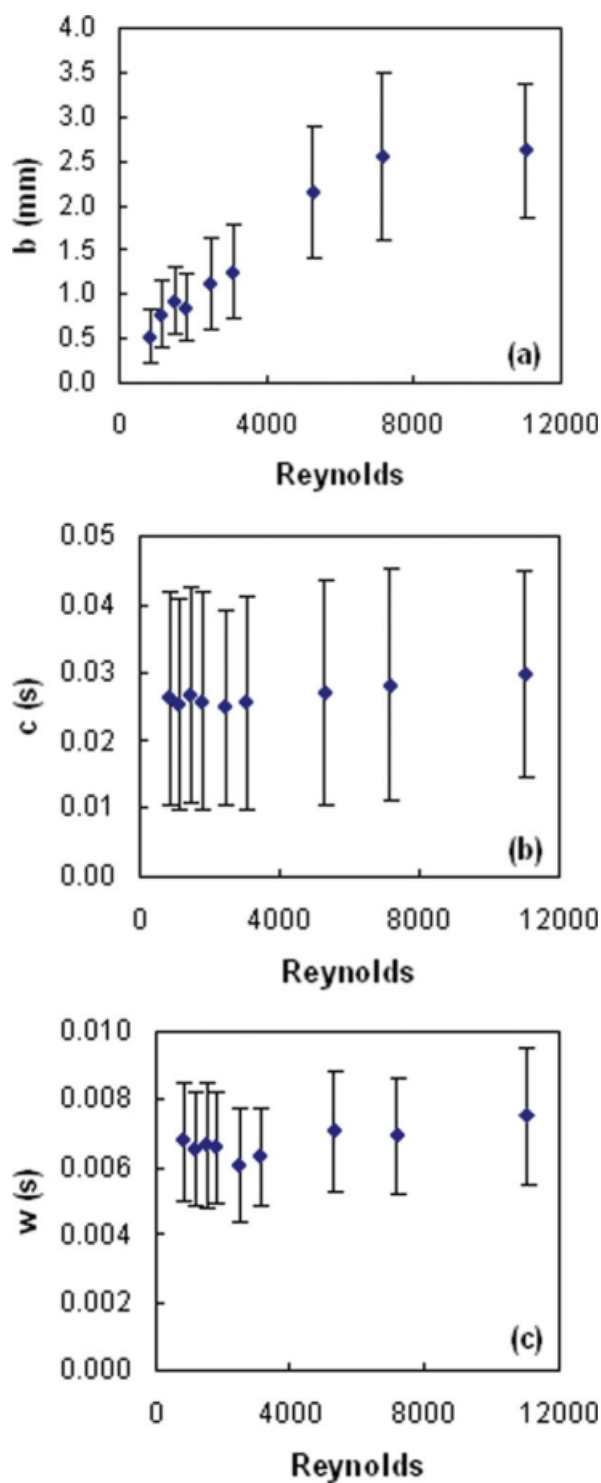


Figure 5. Average value and standard deviation vs.  $Re$  at 2.20 m downstream location of (a) parameter  $b$ , (b) parameter  $c$ , and (c) parameter  $w$ .

[Color figure can be viewed in the online issue, which is available at [www.interscience.wiley.com](http://www.interscience.wiley.com).]

the wave. To transform it to actual length, multiplication by the wave velocity is needed. As it will be shown below, this velocity depends on  $Re$ , so the length of the leading edge of waves also depends on  $Re$ .

It must be noted that although the assumption of uniform PDF for  $b$  (see Touglidis et al.<sup>25</sup>) can be a coarse approximation of the corresponding unimodal PDFs shown in Figure

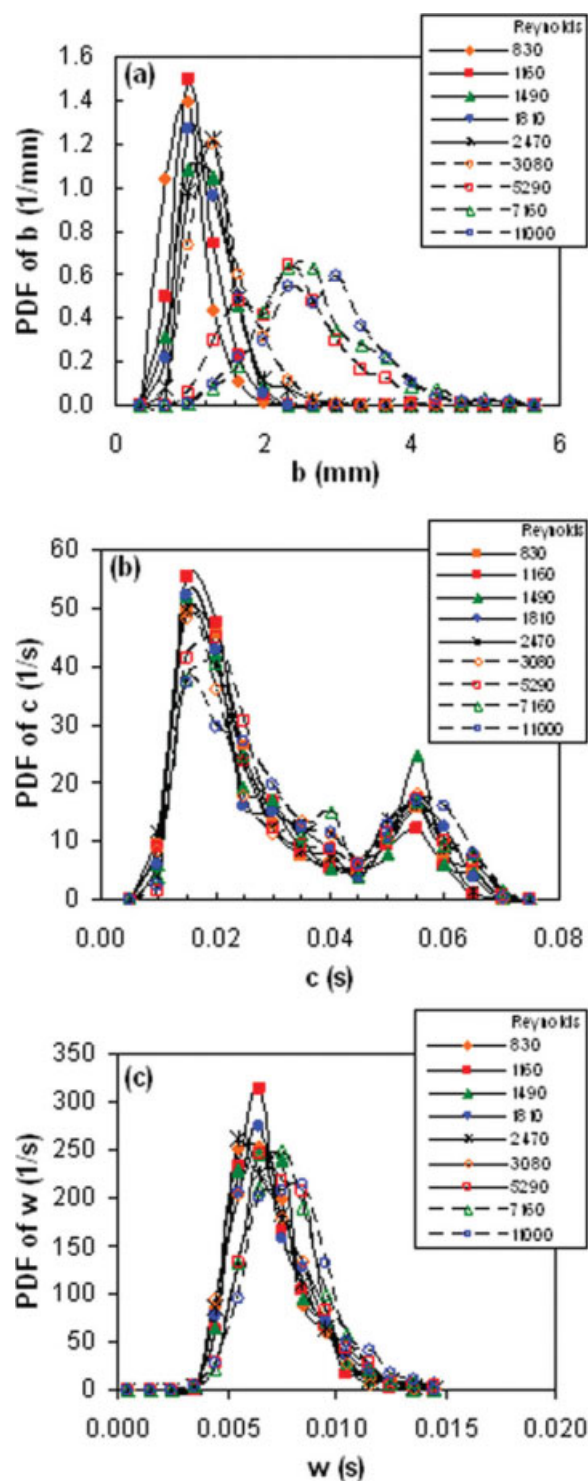
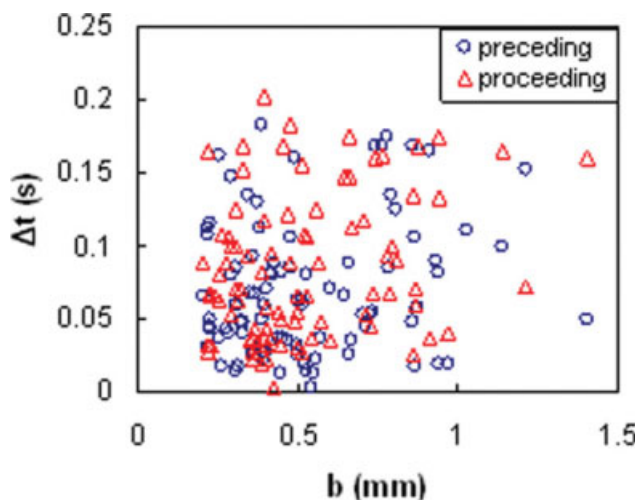


Figure 6. Probability density function for several  $Re$  values of (a) parameter  $b$ , (b) parameter  $c$ , and (c) parameter  $w$ .

[Color figure can be viewed in the online issue, which is available at [www.interscience.wiley.com](http://www.interscience.wiley.com).]



**Figure 7. Typical correlation plot between parameter  $b$  and time interval between the peaks of neighboring waves.**

[Color figure can be viewed in the online issue, which is available at [www.interscience.wiley.com](http://www.interscience.wiley.com).]

6a, the situation is different for parameter  $c$ . The bimodal distributions shown in Figure 6b cannot be approximated by a uniform distribution in any way.

#### Distribution of large waves in time

After the characterization of the static shape of waves, it is desirable to study their relative position within experimental time traces. This type of analysis has not been performed in Tougliadis et al.<sup>25</sup> At first, a relation between the height of a wave and the distance from its neighbors (expressed as the time span between successive wave peaks) is sought. Figure 7 (and many others similar to it) displays the distances between every wave and its preceding and proceeding neighbors vs. their height. It is apparent that there is no correlation between the two quantities. In other words, the size of a wave does not influence its relative position with respect to adjacent waves in a time trace. Next, the time intervals between two successive waves (even waves rejected in the fitting process are considered here to avoid bias of the results) are computed and the corresponding probability density distribution is presented, (Figures 8a–c).

At this point, it must be noted that positioning randomly the waves in a time series corresponds to cutting randomly a line at several points. It is well known that the distribution of line segments in the last problem is given from the solution of breakage equation with uniform kernel and linear breakage frequency.<sup>28</sup> For this particular problem, the solution is the exponential distribution<sup>29</sup> (in terms of statistics it is a Poisson process<sup>30</sup>). Other positioning strategies lead to different distributions. For example, if the breakage (wave positioning) probability does not depend on the segment size, a log normal distribution arises.<sup>31</sup> The PDFs of  $\Delta t$  (constructed by data from all the measurement locations) are presented in Figures 8a–c for several Reynolds number. The shape of the PDFs is alike for Reynolds up to 3080. The long tail of the PDFs shown in Figures 8a, b is characteristic

of the exponential distribution, which denotes random positioning of the waves. The exponential distribution shape is violated at small  $\Delta t$  due to the lower detection limit of the

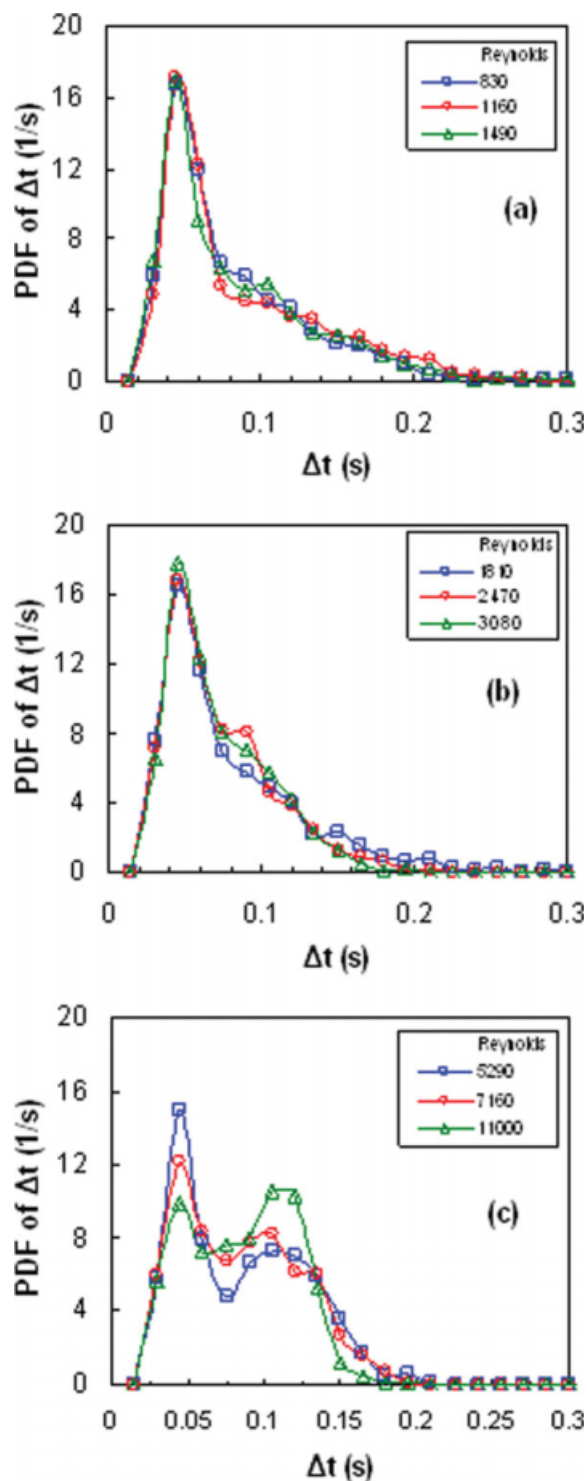


**Figure 8. Probability density functions of the time interval between the peaks of neighboring waves for several  $Re$  values, (a)  $Re = 830, 1160, 1490$ , (b)  $Re = 1810, 2470, 3080$ , and (c)  $Re = 5290, 7160, 11000$ .**

[Color figure can be viewed in the online issue, which is available at [www.interscience.wiley.com](http://www.interscience.wiley.com).]

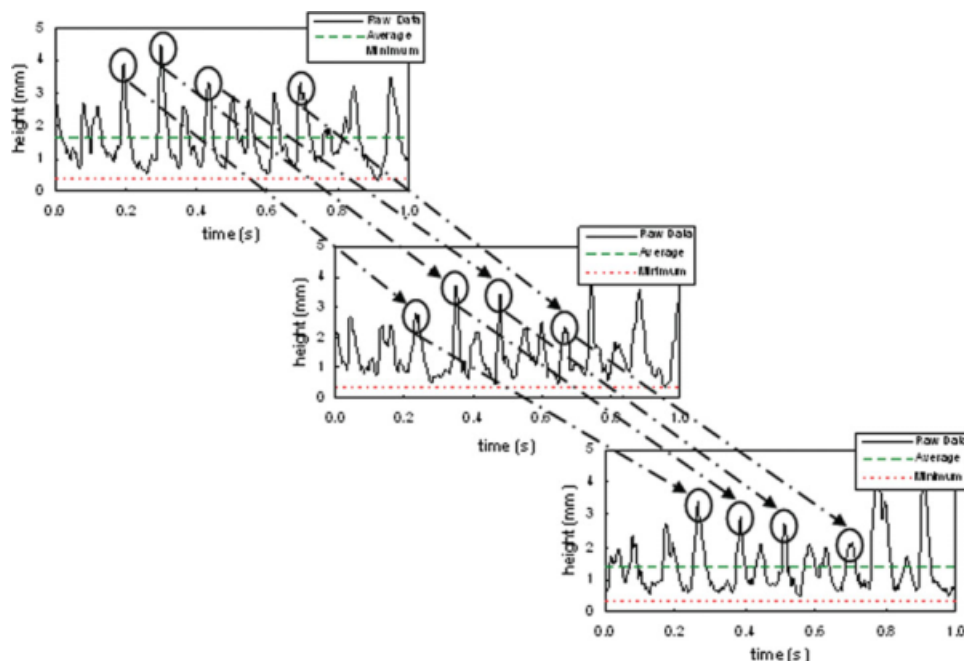


**Figure 9. Procedure of wave identification and evolution tracing from film thickness-time data.**

[Color figure can be viewed in the online issue, which is available at [www.interscience.wiley.com](http://www.interscience.wiley.com).]

process (overlap between waves). The PDF changes its shape at  $Re = 5290$  confirming our previous assertion that the character of the flow changes radically at this point. The PDF becomes bimodal and as the  $Re$  increases the first mode diminishes in favor of the second mode which rises. This implies that the random positioning of waves in the time trace gives its place to an ordered positioning dictated by a mutual repulsion between waves. Actually, the PDF is a static information on the time intervals  $\Delta t$ . Dynamic information such as the sequence in which  $\Delta t$  appears can be in principle analyzed through the use of the Hurst exponent.<sup>32</sup> Unfortunately, for the small sample size of the present data, the corresponding analysis cannot clearly answer the question of existence or persistence in the data.

#### Large wave evolution along the flow

Experimental film thickness traces obtained at several downstream locations allow observations of the evolution not only of average statistical quantities but also of individual waves as they travel with the main flow. The procedure to identify and follow the evolution of individual waves is described next: At first, the thickness-time traces from the different downstream locations are justified in order to achieve coincidence of as many as possible large waves. Practice showed that in our case the coincidence of three major large waves was enough to assure the best possible coincidence of the whole trace, given the stochastic nature of the film surface. This leads to estimation of the average wave velocity between adjacent measuring stations. Each wave found at  $\pm 20$  ms from its expected position based on the estimated average wave velocity is recognized as the evolved state of a wave registered in the preceding (upstream) measuring station. The procedure is shown sche-

matically in Figure 9. There the time traces for three consecutive measurement sites are presented. The circles denote the identification of specific waves and the arrows show their evolution along the flow.

A statistical cross-correlation analysis has been performed for all the traces examined in this work, and in each case, an average wave velocity is computed. The average over all sites cross-correlation velocity is presented with respect to  $Re$  in Figure 10. Also, the average wave velocities estimated

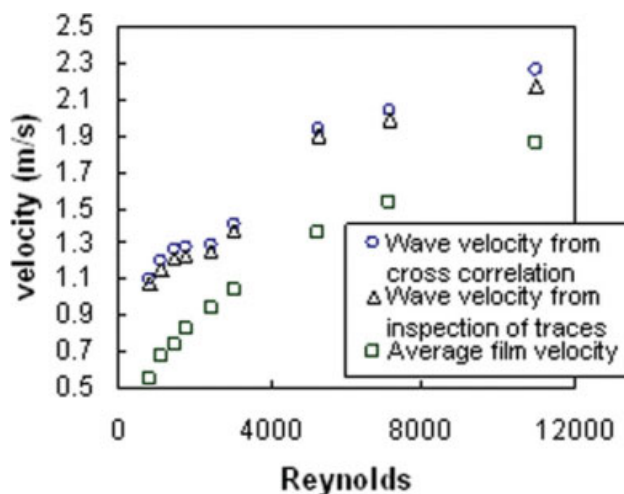


**Figure 10. Average wave velocity from direct data inspection and from statistical cross correlation vs.  $Re$  number.**

The average film velocity is also shown. [Color figure can be viewed in the online issue, which is available at [www.interscience.wiley.com](http://www.interscience.wiley.com).]

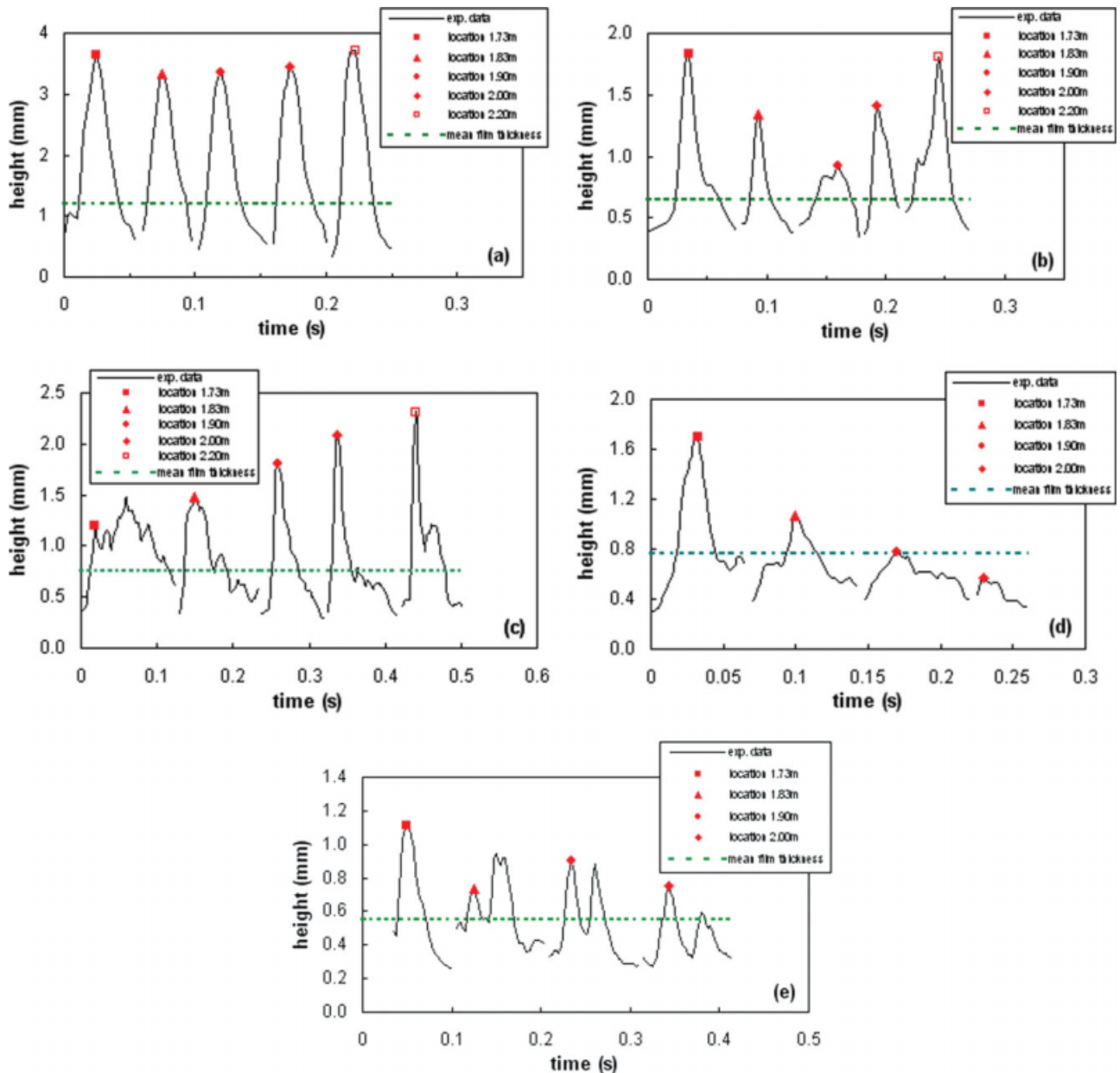


**Figure 11. Downstream typical behaviors of large waves (a) a stable (slightly oscillating) wave ( $Re = 7160$ ), (b) a strongly oscillating wave ( $Re = 2470$ ), (c) wave birth ( $Re = 3080$ ), (d) wave death ( $Re = 3080$ ), and (e) wave splitting ( $Re = 1810$ ).**

[Color figure can be viewed in the online issue, which is available at [www.interscience.wiley.com](http://www.interscience.wiley.com).]

by simple inspection (as described earlier) are shown. The very good agreement between the two sets of data indicates the validity of visual detection. The average velocity of the film is also shown in Figure 10 for comparison.

Having identified and followed all the waves of the traces examined here as they evolve along the flow, it remains to analyze and characterize their behavior. The waves in addition to their simple translation by the flow undergo several size and shape transformations. Typical examples of the most important (frequently observed) transformations are presented in Figure 11. The dominant behavior along the total observation length of this work (about 50 cm) is the

oscillation of the wave around a mean size and shape. Two limiting cases of this behavior are presented in Figures 11a, b, respectively. Figure 11a shows a wave undergoing a small size oscillation almost retaining its shape. On the contrary, a greatly oscillating wave in both size and shape is depicted in Figure 11b. The size of this particular wave drops significantly to slightly above the mean film thickness value of the whole trace (designating its characterization as large wave) before it starts growing up again. However, the oscillation frequency can be larger than the one shown in these figures, going up and down even between two successive measurement sites.

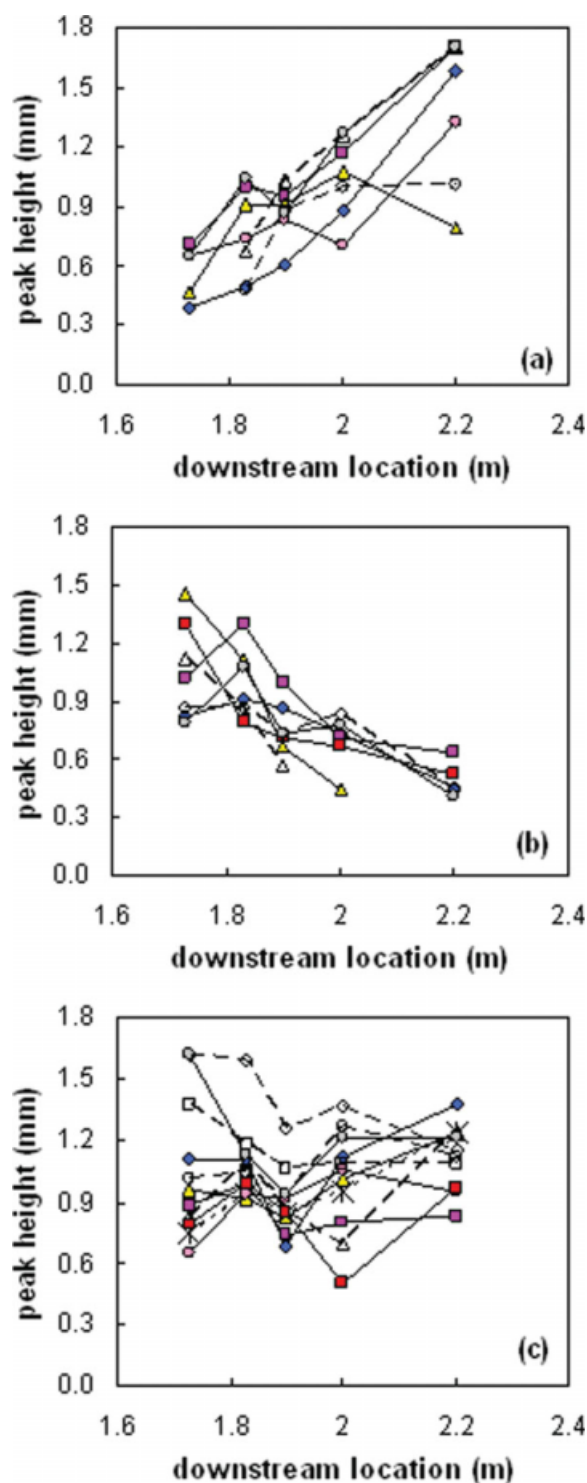


**Figure 12. Downstream evolution of wave peak heights for  $Re = 1160$  (a) emerging waves, (b) decaying waves, and (c) oscillating waves.**

[Color figure can be viewed in the online issue, which is available at [www.interscience.wiley.com](http://www.interscience.wiley.com).]

Another typical behavior observed is the birth (emerge) of large waves. A typical example is shown in Figure 11c. Usually, a large wave is generated by coalescence of smaller

waves as it is shown in the figure. There are two ways in which large waves lose their identity. The first, which is more common, is the simple death (decay) of a wave by decreasing its size along the flow until it disappears (its height gets less than the mean film thickness value). A typical example is shown in Figure 11d. The second way, which is more sporadic, is through splitting into two smaller waves (Figure 11e).

Figure 12 presents the evolution of wave peak height for the particular case of  $Re = 1160$  and for all the emerging waves (Figure 12a), decaying waves (Figure 12b) and for some of the oscillating waves (Figure 12c). It is noted that waves coming from a splitting process are not counted as newly generated waves.

It is interesting to know the relative number of waves emerging, decaying, and oscillating in the data series analyzed in this work. It is understood that the samples are very small for statistically significant results, but it gives an idea of the relative rates of the occurring processes. The percentages of the three categories of observed wave behaviors for the examined  $Re$  numbers is shown in Table 1. In general, the oscillating (stable) waves are far more than those emerging or decaying. Especially for the case of high  $Re$  number, all the waves are simply oscillating with only minor changes in their shape. In some cases, there is a complete match between birth and death events as it is expected for a fully developed flow. In other cases, there is no match due to the small size of the sample (just few birth and death events) and to the splitting effect, which also leads to generation of new waves not considered as birth events.

From the data of this work, a maximum wave birth/death rate of 15 waves/s is estimated (by dividing the number of observed events by the residence time of waves in the observation length) for  $Re$  up to 3000 (with no detectable  $Re$  dependence). It seems that the rate of birth and death events decreases sharply when the Reynolds number exceeds 3000. In fact, for the three largest  $Re$  values examined here no birth/death events are observed between the first and last measurement locations (about 0.25 s residence time of the liquid). This implies that for these  $Re$  numbers the birth/death rate is so small that a longer observation length (residence time) is required for them to be noticed. It must be noted that emerging and decaying large waves contribute only a little (depending on their size) to the dominant wave frequency determined by FFT. So, it is not surprising that the FFT dominant frequency is  $<8$  Hz for all Reynolds numbers.<sup>6,7</sup>

**Table 1. Percentages of Observed Wave Evolution Modes for Several Values of  $Re$  Number**

Reynolds	Births (%)	Deaths (%)	Oscillating (%)
830	4	18	78
1160	16	16	68
1490	9	9	82
1810	8	9	83
2470	5	16	79
3080	3	21	76
5290			100
7160			100
11000			100

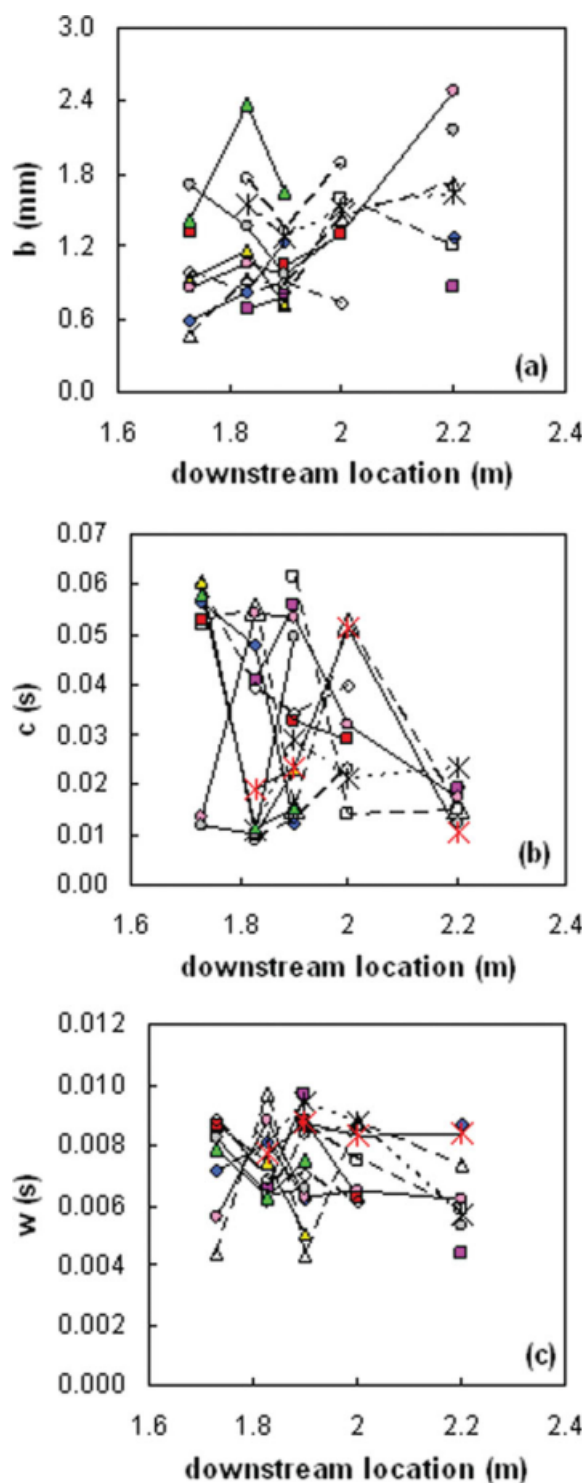


**Figure 13. Downstream evolution of shape parameters for oscillating waves at  $Re = 3080$ : (a)  $b$ , (b)  $c$ , (c)  $w$ .**

[Color figure can be viewed in the online issue, which is available at [www.interscience.wiley.com](http://www.interscience.wiley.com).]

From the above, the most often waves are the oscillating ones. The evolution of the shape parameters  $b$ ,  $c$ ,  $w$  of the oscillating waves for  $Re = 3080$  is shown in Figures 13a–c,

respectively. A similar behavior is observed for all  $Re$  numbers. Missing points from the lines in the plots correspond to waves rejected during the fitting process. The first observation is that there is no clear trend for the change of the shape parameters between successive measurement sites. This means that the correlation length of this evolution procedure is much smaller than the intersite length and cannot be estimated by the present data. Nevertheless, a description of the evolution at a higher scale can be given. It is noted that the oscillation of the wave shape is pretty wild since the intersite distance over which large changes are observed is just a wave length. The relative change of parameter  $c$  from site to site is much larger than those of parameters  $b$  and  $w$ . This is consistent with the very broad bimodal PDF of  $c$ , but it is quite surprising that transition of waves from one mode of PDF of  $c$  to the other mode occurs between two sites.

To quantify the tendency of the parameters of the wave shape to change along the flow, their derivatives with respect to length  $s$  (the distance between measuring stations) are computed. Initially, it seemed more natural to us to take derivatives not with respect to length  $s$  but with respect to the wave residence time ( $s/\text{wave velocity}$ ), which depends on  $Re$  number. The observed trends of the results lead us to abandon the idea of residence time as the length  $s$  dominates the evolution of the wave shape parameters. The PDFs of the derivatives  $\Delta b/\Delta s$ ,  $\Delta c/\Delta s$ ,  $\Delta w/\Delta s$  are unimodal with a close to zero average value (compatible with the observation of constant average properties along the flow). The spread of the PDFs are expressed in terms of the average of the absolute values (a measure similar to standard deviation). These average values of the three derivatives  $\Delta b/\Delta s$ ,  $\Delta c/\Delta s$ ,  $\Delta w/\Delta s$  are shown as functions of  $Re$  number in Figures 14a–c, respectively. It is very important that the rate of change of parameters  $c$ ,  $w$  with respect to flow length is practically independent from the  $Re$  number (as the PDFs of these variables). On the other hand, the rate of change of  $b$  has a  $Re$  dependence similar (but not proportional) to the  $Re$  dependence of the average  $b$  value.

To this end, one may wonder about the origin of the wild oscillations of the shape of the waves along the flow. At this point, one should recall that all theoretical works on the problem assume a 2D geometry ignoring the existing nonuniformity of the flow in third dimension. The only work where the focus is on the three dimensionality of the flow is that by Adomeit and Renz,<sup>26</sup> in which a discussion is made about the relative magnitude of the terms in the Navier-Stokes equation. According to the above work, film thickness is strongly nonuniform in the transverse direction. Taking into account that wild-wave shape oscillations cannot be predicted by 2D theories, they might be just the reflection of the 3D character of the flow to a 2D plane of measurement.

All the above information constitutes essential information regarding the reconstruction of the interface shape of the film. Compared with Touglidis et al.,<sup>25</sup> we have not only improved the static representation of large waves providing detailed and accurate statistical data but also examined the dynamics of waves' distribution and evolution along the flow. The latter is very important as the shape of the

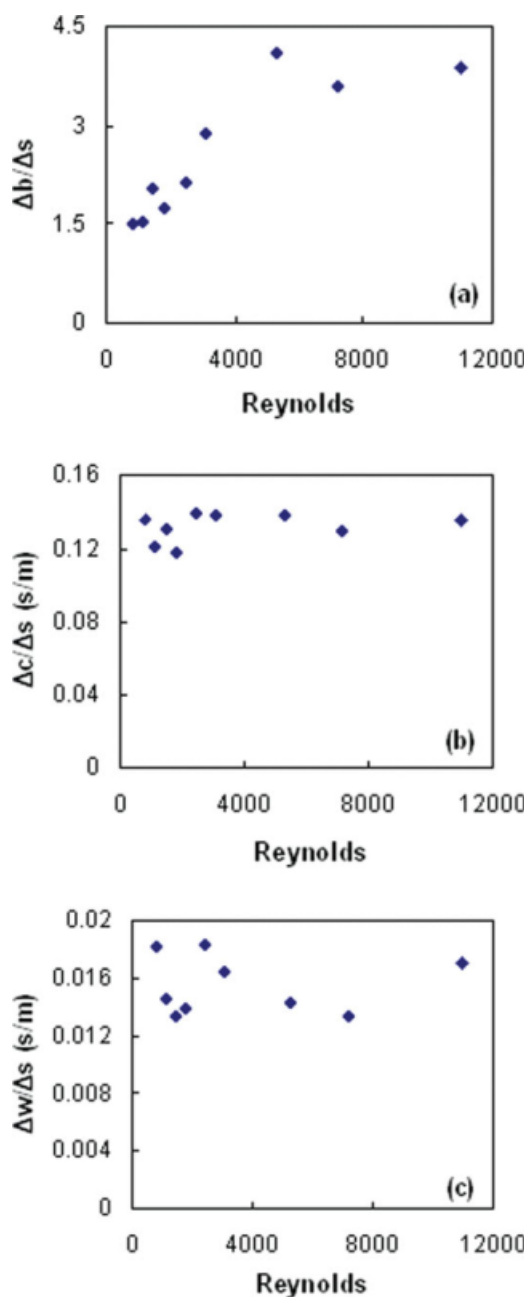


**Figure 14. Slope of the wave shape parameters with respect to length  $s$  along the flow as a function of  $Re$  number (a)  $\Delta b/\Delta s$ , (b)  $\Delta c/\Delta s$ , (c)  $\Delta w/\Delta s$ .**

[Color figure can be viewed in the online issue, which is available at [www.interscience.wiley.com](http://www.interscience.wiley.com).]

interface of turbulent wavy falling films is by no means stationary but evolves in both time and space.

## Conclusions

By analyzing time traces of falling film thickness data obtained at various Reynolds numbers and at several locations along the flow in the region of fully developed flow it was found that:

(1) The large waves shape can be represented by a particular function employing three parameters  $b$ ,  $c$ , and  $w$ . The PDF of  $b$  is unimodal and strongly dependent on  $Re$ , the PDF of  $c$  is bimodal and can be approximately considered as not depending on  $Re$ , and the PDF of  $w$  is unimodal and clearly not depending on  $Re$ .

(2) Large waves are randomly placed in the time traces for  $Re < 3000$ . For  $Re > 5000$ , a mutually repulsion between the waves is observed, which increases as  $Re$  increases.

(3) The motion of large waves along the flow can be considered as a population dynamics process. The waves undergo shape and size transformation (oscillations), splitting or death during their downstream travel. In addition, new large waves are generated from the growth of lower (than the mean film thickness) waves. From the above, the oscillation of waves around a mean shape and size is the most frequently observed event. This is completely unexpected according to 2D theories and indicates a 3D character of the flow. The rate of oscillation of parameters  $c$  and  $w$  with respect to the flow length can be considered independent from  $Re$  number.

The observations and data analysis of this work helps to compress the information taken from the film thickness data with respect to wave dynamics and sets the basis for improving previous efforts for the reconstruction of the film interface shape, e.g., Touglidis et al.<sup>25</sup>

## Acknowledgments

Financial support by the European Space Agency through the project CBC (Convective Boiling and Condensation) (ESA-AO-2004-PCP-111/ELIPS-2) is gratefully acknowledged. This work is conducted under the umbrella of the COST P21 action: Physics of Droplets.

## Literature Cited

1. Collier JG. *Convective Boiling and Condensation*. London: McGraw-Hill, 1972.
2. Karapantsios T, Kostoglou M, Karabelas AJ. Local condensation rates of steam/air mixtures in direct contact with a falling liquid film. *Int J Heat Mass Transfer*. 1995;38:779–794.
3. Kapitza PL. Wave flow of a thin viscous fluid layer. *Zh Eksp Teor Fiz*. 1948;18:1–8.
4. Zhang JT, Peng XF, Peterson GP. Experimental investigation on the hydrodynamics of falling liquid film flow by nonlinear description procedure. *Int J Heat Mass Transfer*. 2000;43:3847–3852.
5. Takahama H, Kato S. Longitudinal flow characteristics of vertically falling liquid films without concurrent gas flow. *Int J Multiphase Flow*. 1980;6:203–215.
6. Karapantsios TD, Paras SV, Karabelas AJ. Statistical characteristics of free falling films at high Reynolds numbers. *Int J Multiphase Flow*. 1989;15:1–21.
7. Karapantsios TD, Karabelas AJ. Longitudinal characteristics of wavy falling films. *Int J Multiphase Flow*. 1995;21:119–127.
8. Ambrosini W, Forgiione N, Oriolo F. Statistical characteristics of a water film falling down a flat plate at different inclinations and temperatures. *Int J Multiphase Flow*. 2002;28:1521–1540.
9. Alekseenko SV, Nakoryakov VY, Pokusaev BG. Wave formation on vertical falling liquid film. *AIChE J*. 1985;31:1446–1460.
10. Mudawwar I, Houtp RA. Measurements of mass and momentum transport in wavy laminar falling liquid films. *Int J Heat Mass Transfer*. 1993;36:4151–4162.
11. Wasden FK, Dukler AE. Insights into the hydrodynamics of free falling wavy films. *AIChE J*. 1989;35:187–195.

12. Salamon TR, Armstrong RC, Brown RA. Traveling waves on vertical films: numerical analysis using the finite element method. *Phys Fluids*. 1994;6:2202–2220.
13. Ramaswamy B, Chippada S, Joo SW. A full-scale numerical study of interfacial instabilities in thin-film flows. *J Fluid Mech*. 1996;325:163–194.
14. Malamataris N, Papanastasiou TC. Unsteady free surface flows on truncated domains. *Ind Eng Chem Res*. 1991;30:2211–2219.
15. Malamataris NA, Vlachogiannis M, Bontozoglou V. Solitary waves on inclined films: flow structure and binary interactions. *Phys Fluids*. 2002;14:1082–1094.
16. Benney BJ. Long waves and liquid films. *J Math Phys*. 1996;45:150.
17. Chang HC, Demekhin EA, Kalaidin E. Simulation of noise-driven wave dynamics on a falling film. *AIChE J*. 1996;42:1553–1568.
18. Yu LQ, Wasden FK, Dukler AE, Balakotaiah V. Nonlinear evolution of waves on falling films at high Reynolds numbers. *Phys Fluids*. 1995;7:1886–1902.
19. Kunugi T, Kino C. DNS of falling film structure and heat transfer via MARS method. *Comput Struct*. 2005;83:455–462.
20. Kunugi T, Kino C, Serizawa A. Surface wave structure and heat transfer of vertical liquid film flow with artificial oscillation. In *5th International Symposium of Multiphase flow, Heat Mass Transfer and Energy Conversion*, Xian, China, 3–6 July, 2005.
21. Dietze GF, Leefken A, Kneer R. Investigation of the backflow phenomenon in falling liquid films. *J Fluid Mech*. 2008;595:435–459.
22. Malamataris NA, Balakotaiah V. Flow structure underneath the large amplitude waves of a vertically falling film. *AIChE J*. 2008;54:1725–1740.
23. Mudawwar IA, El-Masri MA. Momentum and heat transfer across freely-falling turbulent liquid films. *Int J Multiphase Flow*. 1986;12:771–790.
24. Ye H, Yan W, Jiang Z, Li C. Hydrodynamics of free-falling turbulent wavy films and implications for enhanced heat transfer. *Heat Transfer Eng*. 2002;23:48–60.
25. Touglidis LG, Karapantsios TD, Vlachos N, Balouktsis AI. Surface morphology reconstruction of free falling films at high Reynolds numbers. *Int J Multiphase Flow*. 2004;30:351–368.
26. Adomeit P, Renz U. Hydrodynamics of three dimensional waves in laminar falling films. *Int J Multiphase Flow*. 2000;26:1183–1208.
27. Karapantsios TD, Karabelas AJ. Surface characteristics of roll waves on free falling films. *Int J Multiphase Flow*. 1990;16:835–852.
28. Tenchov BG, Yanev TK. Weibull distribution of particle sizes obtained by uniform random fragmentation. *J Colloid Interface Sci*. 1986;111:1–7.
29. Kostoglou M. The linear breakage equation: from fundamental issues to numerical solution techniques. In: *Handbook of Powder Technology*, Vol. 12: *Particle Breakage*. Amsterdam: Elsevier, 2008;793–835.
30. Brown RC. The pore size distribution of model fibers produced by random fragmentation described in terms of the Weibull distribution. *Chem Eng Sci*. 1994;49:145–146.
31. Kolmogoroff AN. The logarithmically normal law of distribution of dimensions of particles broken into small parts. *Dokl Akad Nauk USSR*. 1941;31:99–104.
32. Feder J. *Fractal*. New York: Plenum, 1988.

Manuscript received Dec. 23, 2008, and revision received May 25, 2009.